Author accepted version. Final publication as:
Perez-Alvarado, A., Mydlarski, L.M., Gaskin, S.J. (2016) Effect of the driving algorithm on the turbulence generated by a random jet array, Experiments in Fluids, 57(2): 1-15. doi:10.1007/s00348-015-2103-7

Effect of the driving algorithm on the turbulence generated by a random jet array

Alejandro Pérez-Alvarado

Department of Mechanical Engineering, McGill University, 817 Sherbrooke St. W., Montreal, QC H3A 0C3, Canada

alejandro.perez2@mail.mcgill.ca

Laurent Mydlarski

Department of Mechanical Engineering, McGill University, 817 Sherbrooke St. W., Montreal, QC H3A 0C3, Canada

laurent.mydlarski@mcgill.ca

Susan Gaskin

Department of Civil Engineering and Applied Mechanics, McGill University, 817 Sherbrooke St. W., Montreal, QC H3A 0C3, Canada
susan.gaskin@mcgill.ca

Different driving algorithms for a large random jet array (RJA) were tested and their performance characterized by comparing the statistics of the turbulence generated downstream of the RJA. Of particular interest was the spatial configuration of the jets operating at any given instant (an aspect that has not been documented in previous RJAs studies), as well as the statistics of their respective on/off times. All algorithms generated flows with non-zero skewnesses of the velocity fluctuation normal to the plane of the RJA (identified as an inherent limitation of the system resulting from the unidirectional forcing imposed from only one side of the RJA), and slightly super-Gaussian kurtoses of the velocity fluctuations in all directions. It was observed that algorithms imposing spatial configurations generated the most isotropic flows, however they suffered from high mean flows and low turbulent kinetic energies. The algorithm identified as RANDOM generated the flow that, on an overall basis, most closely approximated zero-mean-flow homogeneous isotropic turbulence, with variations in horizontal and vertical homogeneities of RMS velocities of no more than ±6%, deviations from isotropy (w_{RMS}/u_{RMS}) in the range of 0.62-0.77, and mean flows on the order of 7% of the RMS velocities (determined by averaging their absolute values over the three velocity components and three downstream distances). A relatively high turbulent Reynolds number ($Re_T = u_T \ell/\nu = 2360$, where ℓ is the integral length scale of the flow and u_T is a characteristic RMS velocity) was achieved using the RANDOM algorithm and the integral length scale ($\ell = 11.5$ cm) is the largest reported to date. The quality of the turbulence in our large facility demonstrates the ability of RJAs to be scaled-up and to be the laboratory system most capable of generating the largest quasi-homogeneous isotropic turbulent regions with zero mean flow.

Author accepted version. Final publication as:
Perez-Alvarado, A., Mydlarski, L.M., Gaskin, S.J. (2016) Effect of the driving algorithm on the turbulence generated by a random jet array, Experiments in Fluids, 57(2): 1-15. doi:10.1007/s00348-015-2103-7

I. Introduction

Although turbulent flows are, in general, neither homogeneous nor isotropic, the study of homogeneous isotropic turbulence plays a fundamental role in furthering our understanding of the physics of turbulent flows, as it is the simplest realization of the latter. An important advantage of studying homogenous isotropic turbulence is that it isolates the self-interaction of turbulent fluctuations (Orszag, 1977), and avoids complications arising from additional processes encountered in natural and man-made flows, such as density stratification, mean shear and the effects of fluid-solid boundaries (Tsinober, 2004). Consequently, homogeneous isotropic turbulent flows are often used to study the fundamental properties and mechanisms of turbulence (e.g. internal intermittency, spectral energy transfer). Despite the fact that homogeneous isotropic turbulence is a (relatively) simple flow, it can be difficult to create in the laboratory, since mean velocity gradients are generally necessary for the initial production of turbulent kinetic energy.

To date, the most commonly studied homogeneous isotropic turbulent flow has been grid-generated wind tunnel turbulence, which can achieve relatively high Reynolds numbers, given recent advances such as the development of active grids (Makita, 1991; Mydlarski and Warhaft, 1996) and low-viscosity-fluid wind tunnels (Bodenschatz *et al.* 2014). However, the existence of a mean flow in such arrangements can present a problem in certain situations. For example, Lagrangian measurements in such experimental setups require moving the apparatus with the mean flow, an impractical condition for a variety of reasons (e.g. the need to translate camera systems, the requirement of long flow facilities to follow a stream for a relatively long time interval). These impracticalities can be overcome by utilizing zero-mean-flow turbulence. Moreover, homogeneous isotropic turbulence with zero mean flow permits the study of the fluctuating components of the velocity (and their ensuing effects in phenomena such as turbulent scalar transport, mixing and particle dispersion) in isolation. The generation of three-dimensional homogeneous isotropic turbulence with zero-mean flow has been attempted using diverse novel systems, the first of which involved one, or two, parallel grids (separated by certain distance) oscillating in the direction normal to the plane of the

grids (Thomson and Turner, 1975; McDougall, 1979; Brumley and Jirka, 1987; De Silva and Fernando, 1994; Villermaux *et al.* 1995; Srdic *et al.* 1996; Shy *et al.* 1997; Ott and Mann, 2000; McKenna, 2004; Blum *et al.* 2010; and Blum *et al.* 2011). Although, the optimal mesh sizes, strokes and frequencies of the grid's oscillation have been proposed, the flows generated by this type of system suffer from large mean flows (with the minimum values of mean flows being approximately 25% of the root-mean-square (RMS) velocities, and maximum values of 60% and 30% for single and double oscillating grids, respectively). Additionally, the oscillation of the grid is accomplished by coupling the grid to a mechanical system driven by a motor, thus making it more difficult to build large experimental setups for experiments at high Reynolds numbers.

Another approach to generating nearly zero-mean-flow homogeneous isotropic turbulence has been to place loudspeakers pointing towards the center of a chamber (Hwang and Eaton, 2004; Webster *et al.* 2004; Warnaars *et al.* 2006; Lu *et al.* 2008; Goepfert *et al.* 2010; and Chang *et al.* 2012), with the locations of the speakers obeying symmetry with respect to the chamber's center. Typically the loudspeakers push fluid through circular orifices to generate pulsed (synthetic) jets and induce vortex rings. Although the quality of the turbulent flow is better than that generated by oscillating grids (very low mean flows that are approximately isotropic), the desired flow is confined to a small region in the center of the chamber. For example, Chang *et al.* (2012), with the use of 32 loudspeakers, were able to generate an almost zero-mean-flow homogeneous isotropic turbulence at the center of a chamber with a Taylor-microscale Reynolds number (Re_λ) of approximately 480. However, the central (isotropic) volume of this flow covered a radius of only 5 cm. A similar method to create such flows uses symmetrically placed propellers pointing towards the center of a chamber containing a fluid (Fallon and Rogers, 2002; Birouk *et al.* 2003; De Jong *et al.* 2009; and Zimmermann *et al.* 2010). Again, the homogeneity and isotropy of the flow ends up being limited to a small central region.

Symmetrically arranged rotating elements have also been employed to achieve zero-mean-flow turbulence. Rotating grids (Liu *et al.* 1999) and propellers (Berg *et al.* 2006) have been used to create homogeneous isotropic turbulent flow

in the center of a rectangular tank. However the levels of turbulence were modest ($Re_\lambda \sim 290$ and 172, respectively) and the isotropic flow was limited to a central volume of approximately $4\times4\times4$ cm^3. Two counter-rotating disks in cylindrical containers have been widely used (introduced by Douady *et al.* 1991 and further used by Fauve *et al.* 1993; Maurer *et al.* 1994; Cadot *et al.* 1995; Belin *et al.* 1996; Aumaitre *et al.* 2000; Mordant *et al.* 2001; and Voth *et al.* 2002). Due to the physical characteristics of this type of system, it generates a cylindrical region of turbulence, with axial extension depending on the size of the tank (e.g. Machicoane *et al*. (2014), and references therein), negligible mean flow and relatively high Re_λ (Voth *et al.* (2002) reached Re_λ=970.) However, the flow suffers from anisotropy and the radial extent of the optimal flow covers only a few centimeters. In a modification of this technique Liberzon *et al.* (2005) used eight counter-rotating disks to generate the turbulence. However, the flow generated at the center of their tank had a low Reynolds number ($Re_\lambda \sim 40$).

Random jet arrays (RJAs) are relatively new systems that have been developed and used to generate approximately homogeneous isotropic turbulence with zero mean flow (Variano *et al.* 2004; Lavertu, 2006; Variano and Cowen, 2008; Delbos *et al.* 2009; Khorsandi *et al.* 2013; and Bellani and Variano, 2014). A (single) RJA is a planar configuration of jets that, randomly and independently, turn on and off to produce turbulence downstream of the array. The RJA is able to create a nearly homogenous flow (albeit with an unavoidable decay in the direction normal to the plane of the jets) with a negligible mean flow (less than 10% of the RMS velocities in all directions) over a large spatial region (Variano and Cowen, 2008). Additionally, the isotropy of the flow is of the same order as that of grid-generated, wind tunnel turbulence and relatively high Reynolds numbers can be reached (Re_λ = 314 in Variano and Cowen, 2008). The isotropy, quantified as the ratio of RMS velocities (i.e. $u_{\alpha\text{-RMS}}/u_{\beta\text{-RMS}}$), measured in mono-planar RJAs (Variano *et al.* 2004 (0.81); Lavertu, 2006 (0.66); Variano and Cowen, 2008 (0.79); Delbos *et al.* 2009 (0.76); Khorsandi *et al.* 2013 (0.71)) can be as low as two-thirds, presumably resulting from the forcing from only one plane. Most recently, Bellani and Variano (2014) placed two RJAs separated by a distance and facing each other. The resulting profile of the turbulent kinetic energy had zero slope at the tank center due to the underlying symmetry of their arrangement. This configuration generated a nearly

homogeneous isotropic turbulent flow with a negligible mean flow at the center of the tank. Using this arrangement, the isotropy was significantly improved (compared to single RJAs) and found to be in the range 0.95-0.99 in the center of the tank. The Taylor-microscale Reynolds number was 334 and the region of homogeneity and isotropy was roughly $0.4\times0.4\times0.2$ m^3 (the largest reported to date).

The present investigation is motivated by the growing interest in random jet arrays as laboratory systems that are the most capable of accurately approximating zero-mean-flow homogeneous isotropic turbulence. The objective of this work is to study different RJA driving algorithms to investigate the statistics of the resulting flow in an attempt to both describe and optimize the characteristics of the generated turbulence, while concurrently identifying the limitations of such systems.

II. Experimental setup

The experiments were carried out in a $1.5\times2.4\times0.9$ m^3 section of a large glass tank ($1.5\times6.0\times0.9$ m^3) in the Environmental Hydraulics Laboratory in the Department of Civil Engineering and Applied Mechanics at McGill University. The tank was filled with water and its top was open to the ambient air.

A planar random jet array was used to produce a turbulent flow in the tank (Figure 1). The three other vertical sides of the measurement region were the side walls, which consisted of panes of tempered glass, as did its bottom. The top of the tank was open to the ambient air, with a free surface of water. The RJA consists of 10 columns of 6 bilge pumps (Rule 25D, 500 GPH) attached to a vertical sheet of high density polyethylene (1 x 1.5 m^2). The jet array is based on that of Variano and Cowen (2008), but built to a larger scale. The jets are equally spaced in the horizontal and vertical directions (with center to center distance, M, of 15 cm) having symmetric boundary conditions, which were chosen to minimize possible secondary flows, in analogy with oscillating grid turbulence (Fernando and De Silva, 1993). The pumps draw water in from their base and discharge it from an outlet oriented perpendicularly to the plane of the jet array – see figure 1(c). Since the suction and discharge occur simultaneously into the same fluid volume, there is

a zero net mass flow rate in a control volume containing the pump, which is essential to generate the zero mean flow in the tank. A 15 cm extension (3.18 cm in diameter) is attached to the outlet of each pump to straighten the flow upon its exit from the pumps. The random jet array is controlled using a custom algorithm programmed in LabVIEW, which independently turns the pumps on and off. Downstream of the jet array, the jets merge, generating a region of turbulence that decays in the direction normal to the plane of the jet array. The independent functioning of each pump allowed us to explore different driving algorithms (section IV) and compare the statistics of the resulting turbulent flows (section V).

Author accepted version. Final publication as:
Perez-Alvarado, A., Mydlarski, L.M., Gaskin, S.J. (2016) Effect of the driving algorithm on the turbulence generated by a random jet array, Experiments in Fluids, 57(2): 1-15. doi:10.1007/s00348-015-2103-7

(a)

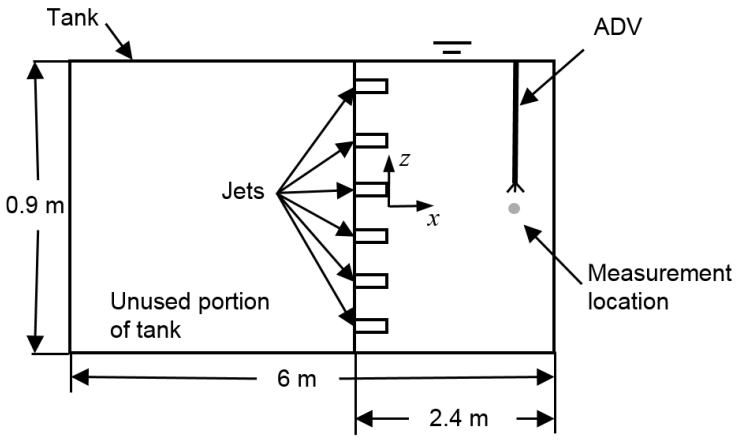

(b)

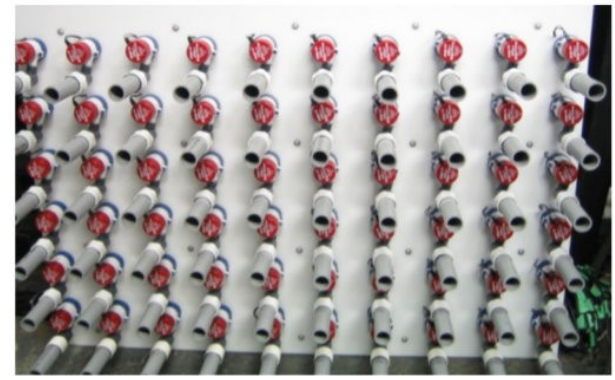

(c)

Figure 1. Experimental facility: (a) schematic of the apparatus: side view (not to scale); (b) a photograph of the random jet array; (c) a close-up, side view of the bilge pumps in which one can observe their inlets (on their blue bottoms) and the gray PVC extensions to their outlets.

Author accepted version. Final publication as:
Perez-Alvarado, A., Mydlarski, L.M., Gaskin, S.J. (2016) Effect of the driving algorithm on the turbulence generated by a random jet array, Experiments in Fluids, 57(2): 1-15. doi:10.1007/s00348-015-2103-7

III. Measurement technique and post-processing

Velocity measurements were obtained using a Nortek Vectrino acoustic Doppler velocimeter (ADV). The ADV probe consists of a central transmitter (which emits short ultrasonic pulses) and four receivers that collect the acoustic signals reflected from particles in the measurement volume. Details of the principles of operation of ADVs can be found in Voulgaris and Trowbridge (1998), McLelland and Nicholas (2000), and the Vectrino Velocimeter User Guide (Nortek, 2004). Given that the ultrasonic pulses do not reflect from clean water, hollow glass microspheres (Potters Industries Sphericel #110P8) with a density (ρ_p) of 1.1 ± 0.05 kg/m^3 were added to the water to increase the ADV's signal-to-noise ratio (SNR). The size distribution of the particles was such that 10% of the particles' diameters (D_p) were smaller than 5 μm, 50% smaller than 10 μm, 90% smaller than 21 μm, and 97% smaller than 25 μm. The minimum acceptable values of the SNR and correlation recommended by the manufacturer are 17 dB and 70%, respectively. Their values are calculated by the Vectrino software for each velocity measurement. The SNR has its usual definition of SNR= $20\log_{10}(\text{Amplitude}_{signal}/\text{Amplitude}_{noise})$ and the correlation is a measure of the similarity of two pulse echoes being measured by the instrument (hence in the range 0-100%). Details of the calculations can be found in the Vectrino Velocimeter User Guide (Nortek, 2004). Sufficient particles were mixed with the water to maintain the values above 20 dB and 97% at all times, ensuring an optimal quality of our measurements. Furthermore, the particles passively followed the flow given their low Stokes number: $St = \tau_0/\tau_\eta$, where $\tau_\eta = (\nu/\varepsilon)^{1/2}$ is the Kolmogorov time scale of the flow (with the dissipation rate of turbulent kinetic energy per unit mass being estimated as $\varepsilon = u^3/\ell$, where ℓ is the integral length scale of the flow) and $\tau_0 = \rho_p D_p^2/(18\mu)$ is the particle response time (where μ=0.001 N·s/m^2 is the dynamic viscosity of water). The Stokes number in the present experiments was within the range 9.4×10^{-9} - 2.3×10^{-7}, well below 1, ensuring that the particles passively followed the flow.

The sampling volume of the ADV is located 5 cm below the probe, thus minimizing flow disturbances, and was set to its maximum volume of 0.42 cm^3. The power level of the ADV was also set to the maximum value. Selecting the maximum values of power and volume results in the highest SNR and correlation for the system. The ADV was connected to a computer that controlled the parameter

settings and data acquisition through the Vectrino software. 2.25×10^5 data points were recorded for each experiment at the ADV's maximum sampling rate of 25 Hz, for a total duration of 2.5 hours. The latter represents 1000 to 3000 integral time scales, depending on the downstream distance from the RJA. A record of this length ensured that statistics up to fourth order (i.e. kurtosis) were converged.

Velocity measurements were taken over a range of distances from the jet array (5.5M - 9.3M) with the probe measurement volume located in the center of the plane parallel to the RJA. The flow in planes parallel to the RJA was measured in Khorsandi (2011) and was shown to be statistically homogeneous at sufficient distances (> 5M) from the individual jets of the RJA due to the symmetry of the apparatus. Figure 2 reproduces two figures from Khorsandi (2011) for one representative driving algorithm ("RANDOM" – see the next section for the details of its operation). Figure 2a) indicates that a horizontal transect of $\langle W \rangle$ is constant to within -0.08 to +0.13 cm/s and that w_{RMS} is constant to within ±6% of its mean value at that location. (Quoting percentages for the mean velocities is not sensible, as their nominal value is zero.) Figure 2b) indicates that $\langle U \rangle$ and $\langle W \rangle$ fall within the ranges -0.19 to +0.11 cm/s and -0.22 to +0.04 cm/s, respectively, and that u_{RMS} and w_{RMS} are constant to within ±5% and ±4% of their respective mean values. Thus the flow generated by the RJA operating using the RANDOM algorithm can be classified as homogeneous, to a reasonable approximation. Full homogeneity tests were not performed for all the 9 algorithms discussed herein. But although the homogeneity of a generated flow may be somewhat algorithm dependent in the near-field, it is reasonable to expect that this dependence should decay with increasing distance from the RJA, as the flow continues to mix and differences in velocity are eliminated, as would be expected given the underlying symmetries of the driving algorithms (to be discussed), and as also demonstrated by Variano and Cowen (2008).

Author accepted version. Final publication as:
Perez-Alvarado, A., Mydlarski, L.M., Gaskin, S.J. (2016) Effect of the driving algorithm on the turbulence generated by a random jet array, Experiments in Fluids, 57(2): 1-15. doi:10.1007/s00348-015-2103-7

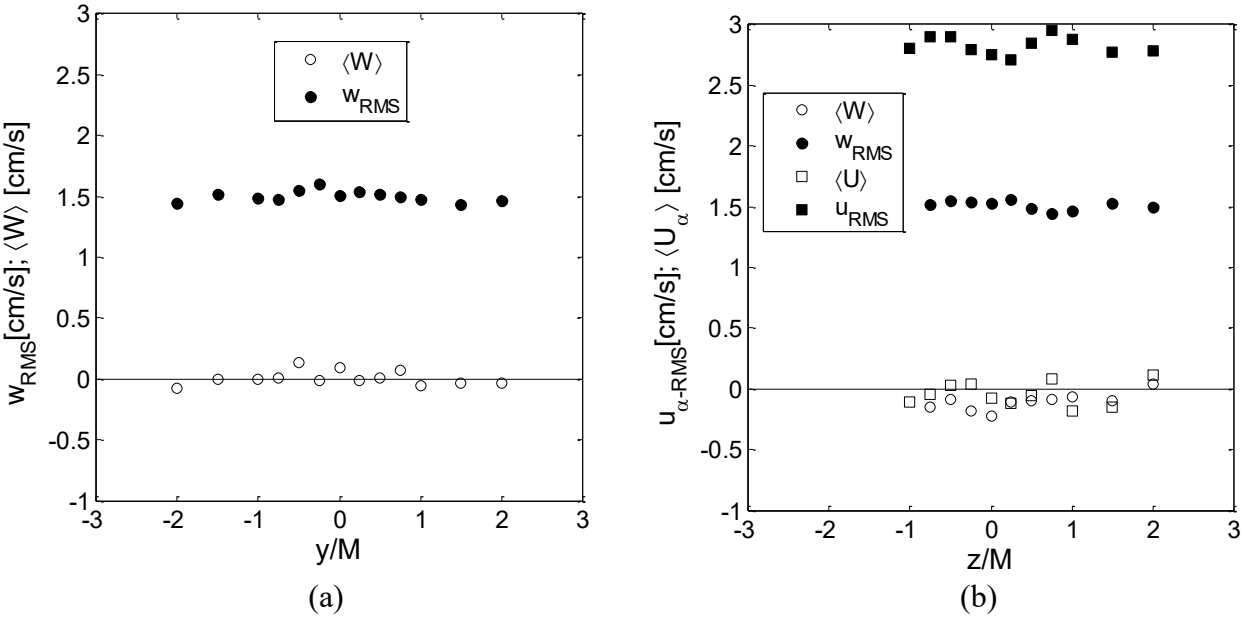

Figure 2. Horizontal and vertical homogeneity for the RANDOM algorithm. (a) ⟨W⟩ and w_{RMS} velocities along a horizontal line passing through z/M = 1.5 measured at x/M = 7.3. (b) ⟨U⟩, ⟨W⟩, u_{RMS} and w_{RMS} velocities along a vertical line passing through y/M = 0. (⟨U⟩ and u_{RMS} measured at x/M = 5.5. ⟨W⟩ and w_{RMS} measured at x/M = 7.3.) Adapted from Khorsandi (2011).

It is known that the *u* and *v* components of the RMS velocity are overestimated by the ADV systems (Voulgaris and Trowbridge, 1998; Khorsandi *et al.* 2012). Due to the geometry of the ADV, the velocities measured by its four receivers are at a very small angle from the transmitter beam, resulting in a higher precision in the *w* component of the velocity (Nortek, 2004). Therefore the probe was oriented such that its measured *v* and *w* components of velocity were located in a plane parallel to the RJA (Figure 1a). This configuration allows the noise correction method for axisymmetric flows of Khorsandi *et al.* (2012) to be applied, correcting the known overestimation in the *u* and *v* components of the RMS velocity. To use the correction method of Khorsandi *et al.* (2012), the ADV probe is oriented so that measured (average) statistics of the *v* and *w* velocities can be assumed to be identical, given the RJA's underlying symmetries. (This assumption was validated by making 3 separate measurements of the 3 components of velocity, each using the ADV oriented in a way that the measurements were made using its highest-precision (*z*) direction. Axisymmetry was confirmed, with the variations in v_{RMS} and w_{RMS} being less than 2% for each of the 3 downstream distances studied

herein, using the RANDOM algorithm, to be discussed shortly.) The excess noise variance in the y-direction can then be inferred by subtracting the variance of w from that of the overestimated variance of v (i.e. $\sigma^2_{\text{v-noise}} = \langle v^2 \rangle - \langle v^2 \rangle_{\text{true}}$, where $\langle v^2 \rangle_{\text{true}} = \langle w^2 \rangle$, and where $\sigma^2_{\text{v-noise}}$ is defined as the noise variance in v, assuming that the true signal and the noise are statistically uncorrelated). The noise variance in v is converted to that of u using the ADV's transformation matrix. The true variance of u is then obtained by subtracting the calculated noise variance in u from the calculated variance in u. The interested reader is referred to Khorsandi (2011) and Khorsandi *et al.* (2012) for more details on this noise correction procedure. (Note the different coordinate system in those references.)

IV. Jet driving patterns

The ability to independently operate and control each jet in the array allowed us to investigate different RJA driving algorithms generating the turbulence. Of particular interest was the spatial configuration of the pumps turned on at any given instant, as well as the statistics of their respective on/off times. Given the results of Variano and Cowen (2008), who found a superior performance of random algorithms over deterministic ones, we focus mainly on driving algorithms that are spatial variations with a random element whose on/off times are randomly selected from normal distributions with their respective mean (μ) and standard deviation (σ). Table 1 summarizes the relevant parameters for each algorithm tested in the present experiments, which are grouped into 4 different classes of algorithms.

Table 1. Summary of algorithm parameters

Group	Algorithm	μ_{on} [s]	σ_{on} [s]	μ_{off} [s]	σ_{off} [s]

1	RANDOM	12	4	108	36
2	4SECTRANDOM1	12	4	108	36
	4SECTRANDOM2	6	1.5	48	12
	4SECTRANDOM3	4	1	32	8
	4SECTRANDOM4	2	0.5	16	4
3	CHESSBOARD	∞	∞	∞	∞
	EQUALCHESS	12	0	12	0
	RANDOMCHESS	12	4	12	4
4	RANDOMNUMBER	Threshold = 0.98; t = 0.4 s			
		20	19.8	20	19.8

The RANDOM algorithm is that used by Khorsandi (2011) and Khorsandi *et al.* (2013). It was proposed in Variano and Cowen (2008) as the "sunbathing" algorithm and its parameters were optimized by both groups. We do not, therefore, investigate any further optimization of this class of algorithm. However, neither group documented the results of other classes of algorithms. When the RANDOM algorithm is used, each pump is independently and randomly turned on and off. The on and off times are random values determined from normal distributions with adjustable mean (μ) and standard deviation (σ). For the RJA used herein, Khorsandi (2011) investigated variations of mean on times (ranging from 3-12 s) and mean off times (ranging from 15 to 108 s) with the standard deviations fixed at 1/3 of the respective mean times (e.g. $\sigma_{on}/\mu_{on} = \sigma_{off}/\mu_{off} = 1/3$). The 1/3 ratio was chosen following the analysis of Variano and Cowen (2008), who found very little sensitivity of the mean flow and RMS velocities to the values of σ_{on} and σ_{off}. In the examination of different mean on and off times, Khorsandi (2011) identified that larger times improved the statistics of the flow. The larger on/off times are presumably required given: i) the size of the facility, and ii) the time required for the turbulence generated by the RJA jets to propagate downstream. Short on/off times fail to sustain an optimal turbulent flow in a large tank since the effects of the turbulence generated by the small injections of momentum rapidly vanish within a short distance from the RJA, and the flows generated by adjacent jets do not spread apart far enough to interact and therefore homogenize the flow.. Khorsandi *et al.* (2013) found that the optimal values for their larger RJA were (μ_{on}, σ_{on}) = (12, 4)

seconds and (μ_{off} , σ_{off}) = (108, 36) seconds, such that, on average, 10% of the pumps are on (or working). We use the same parameters in our investigations of the RANDOM algorithm.

Given the large positive values of the skewness of the *u* velocity measured in the works of Lavertu (2006), Variano and Cowen (2008), and Khorsandi *et al.* (2013), we hypothesized that the RANDOM algorithm may be susceptible to the operation of a single jet (or few adjacent jets), which might cause local, short-term large flows (and hence the large values of skewness). To test this hypothesis a new algorithm named 4SECTRANDOM was proposed and tested. In this algorithm, the RJA is divided into four sections of 3 by 5 pumps (group 2 in Table 1). The jets in a given quadrant (e.g. upper left) were then individually turned on and off over random intervals (in the same fashion as in RANDOM) and the rest of the quadrants turned their pumps on and off to obey (odd) symmetry (in both the *y* and *z* directions) with respect to the center of the RJA to ensure a statistically homogeneous distribution of working pumps. In other words, the "master" quadrant independently and randomly turned on the jets while the other three "slave" quadrants operated their jets in a manner that would enforce symmetry. Figure 3 shows an instantaneous state of the jet array using an algorithm of the class 4SECTRANDOM. Different on and off times were tested under this conditions (see Table 1).

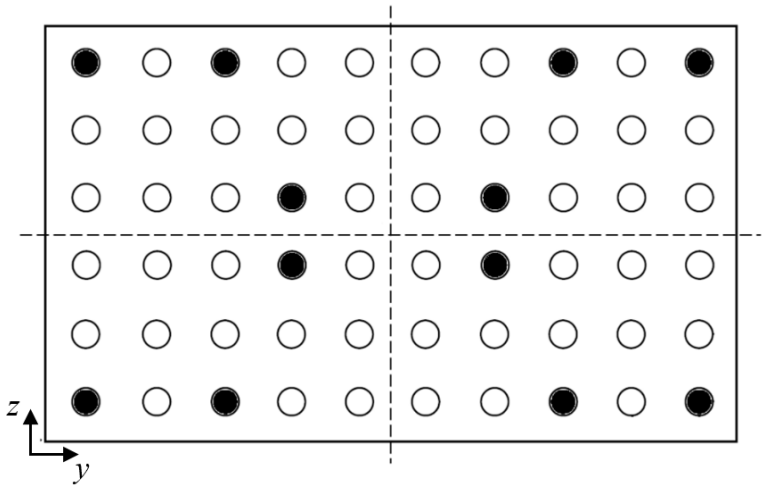

Figure 3. Example of a given instantaneous state of the planar array using the 4SECTRANDOM algorithms (front view). Filled circles represent jets turned on. At this instant, three jets are on in the "master" (upper left) quadrant and the other three "slave" quadrants turn their jets on to enforce symmetry with respect to the center.

To further investigate the effect of the spatial distributions of operating jets, less intermittent patterns were also explored. In the CHESSBOARD algorithm (group 3 in Table 1), 50% of the pumps were on at all times following the pattern depicted in Figure 4. The EQUALCHESS algorithm changed the state of all jets (from on to off and vice versa) in a chessboard distribution every 12 seconds. And the RANDOMCHESS algorithm changed the state of the chessboard at intervals determined from a normal distribution with mean (μ) of 12 seconds and standard deviation (σ) of 4 seconds. The latter algorithm decouples the random nature of the forcing in space and time, by having a deterministic forcing in space, but a random one in time. The mean on times and standard deviation in the chess-like algorithms were selected as 12 and 4 seconds, respectively – the same values as used in the RANDOM algorithm. This served to isolate the effect of the spatial distribution of the operating jets on the generated turbulence.

Finally, inspired by the functioning of an active grid, the RANDOMNUMBER algorithm turned the jets on and off independently if a random number (between 0 and 1) generated for each pump was greater than a certain threshold (0.98). A new random number was generated every 0.4 seconds. The threshold and the period for the random number generation are taken in analogy

with the active grid operation of Mydlarski and Warhaft (1998), which has similar characteristics to a RJA (i.e. varying open and closed portions, resulting in discrete jets), as well as similar dimensions (a mesh of 8 x 8 winglets in a wind tunnel of 0.9 x 0.9 m^2 cross section).

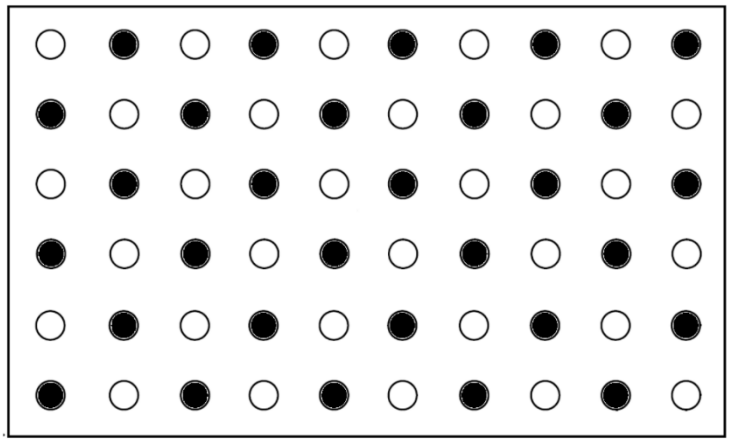

Figure 4. Chessboard spatial distribution of jets (front view).

V. Results

In this section the statistics of the turbulent flows generated by the different algorithms are compared to i) characterize the differences that result from the variation of driving patterns, and ii) identify the optimal algorithm for the production of high-Reynolds-number, homogeneous, isotropic zero-mean-flow turbulence. An "optimal" algorithm is defined as one that generates turbulence with the lowest possible mean flow ($\langle U\rangle/u_{RMS}$, $\langle V\rangle/v_{RMS}$, $\langle W\rangle/w_{RMS} << 1$), high degrees of isotropy ($u_{RMS} \approx v_{RMS} \approx w_{RMS}$; $S_u = S_v = S_w = 0$; and $K_u = K_v = K_w$) and (ideally) high RMS velocity. Measurements at different downstream positions (x/M) from the RJA were performed (for each algorithm) to quantify the decay of the generated turbulence. Table 2 presents the results at different measurement positions for all the algorithms tested. It is important to mention that measurements at x/M=9.3 were not performed for some algorithms due to the low levels of turbulence generated at that farthest downstream location.

Author accepted version. Final publication as:
Perez-Alvarado, A., Mydlarski, L.M., Gaskin, S.J. (2016) Effect of the driving algorithm on the turbulence generated by a random jet array, Experiments in Fluids, 57(2): 1-15. doi:10.1007/s00348-015-2103-7

Table 2. Measurement position, mean flow, RMS velocity components, isotropy, skewness, kurtosis and turbulent kinetic energy (TKE) for the different algorithms tested.

Algorithm	x/M	⟨U⟩ [cm/s]	⟨V⟩ [cm/s]	⟨W⟩ [cm/s]	u_{RMS} [cm/s]	$v_{RMS}=w_{RMS}$[1] [cm/s]	⟨U⟩/u_{RMS}	⟨V⟩/v_{RMS}	⟨W⟩/w_{RMS}	w_{RMS} / u_{RMS}	S_u	S_v	S_w	K_u	K_v	K_w	TKE [cm^2/s^2]
Group 1 RANDOM	5.5	-0.02	-0.11	-0.15	3.06	1.90	-0.01	-0.06	-0.08	0.62	1.09	0.2	0.13	4.60	4.61	4.15	8.28
	6.7	-0.01	0.04	-0.08	2.65	1.67	0	0.03	-0.05	0.63	1.26	0.04	0.08	5.05	4.62	4.02	6.31
	9.3	-0.31	0.04	-0.23	1.55	1.20	-0.2	0.03	-0.19	0.77	1.42	0.15	0.33	6.72	5.02	4.38	2.64
Group 2 4SECTRANDOM1	5.5	0.24	0.18	-0.30	4.18	1.67	0.06	0.11	-0.18	0.40	1.5	0.28	0.18	5.65	5.60	4.35	11.54
	6.7	0.39	0.15	-0.13	3.47	1.62	0.11	0.09	-0.08	0.47	1.49	0.17	0.33	5.71	5.58	4.73	8.62
	9.3	0.34	0.01	-0.15	2.22	1.21	0.15	0.01	-0.12	0.55	1.84	-0.13	0.45	7.81	6.08	5.22	3.92
4SECTRANDOM2	5.5	-0.13	-0.17	-0.05	2.18	1.38	-0.06	-0.13	-0.04	0.64	1.42	0.29	0.28	6.33	5.40	4.84	4.28
	6.7	0.13	0.11	0.06	1.95	1.23	0.07	0.09	0.05	0.63	1.59	0.09	0.43	6.70	6.60	4.87	3.41
	9.3	-0.09	-0.07	0.06	1.02	0.72	-0.09	-0.1	0.09	0.71	1.86	-0.28	0.52	9.08	5.93	5.00	1.03
4SECTRANDOM3	5.5	-0.85	-0.55	0.09	1.49	0.99	-0.57	-0.55	0.09	0.67	1.7	0.45	0.30	8.60	7.15	5.89	2.10
	6.7	-0.06	0.07	-0.03	1.44	0.92	-0.04	0.08	-0.04	0.64	1.72	0.15	0.41	7.58	7.85	5.16	1.89
	9.3	-0.38	0.05	0.04	0.59	0.53	-0.65	0.09	0.07	0.89	1.41	-0.2	0.49	7.78	6.03	5.70	0.45
4SECTRANDOM4	5.5	0.17	0.09	-0.15	1.50	0.87	0.12	0.1	-0.18	0.58	1.69	0.16	0.37	8.51	9.99	7.31	1.88
	6.7	-0.22	-0.04	-0.15	1.02	0.65	-0.21	-0.06	-0.24	0.64	1.91	-0.07	0.59	9.45	8.26	7.16	0.94
Group 3 CHESSBOARD	5.5	0.52	1	0.42	1.51	1.28	0.34	0.78	0.33	0.85	0.85	0.26	-0.23	4.42	4.69	3.90	2.77
	6.7	0.23	0.64	0.10	1.17	0.87	0.19	0.73	0.12	0.75	1.07	0.33	0.02	4.91	4.83	3.49	1.45
EQUALCHESS	5.5	-0.46	0.71	0.47	1.44	1.02	-0.32	0.7	0.46	0.71	1.65	-0.03	0.27	7.50	6.02	4.91	2.08
	6.7	-0.99	0.67	0.33	0.57	0.70	-1.75	0.95	0.46	1.24	0.68	-0.19	0.12	6.29	3.35	3.14	0.66
RANDOMCHESS	5.5	-0.48	0.57	0.29	1.40	1.01	-0.34	0.57	0.29	0.72	1.58	0.17	0.35	7.27	5.64	4.66	1.99
	6.7	-0.89	0.79	0.45	0.75	0.76	-1.19	1.04	0.59	1.01	1.16	-0.28	0.08	8.53	3.83	3.41	0.86
Group 4 RANDOMNUMBER	5.5	-0.5	0.32	-0.23	2.70	1.81	-0.18	0.18	-0.13	0.67	1.29	0.02	0.13	5.11	4.69	3.98	6.91
	6.7	-0.77	0.18	-0.18	1.91	1.40	-0.4	0.13	-0.13	0.73	1.49	-0.21	0.28	6.43	4.85	4.18	3.79
	9.3	-0.66	0.09	-0.10	1.06	1.08	-0.63	0.09	-0.09	1.02	0.82	-0.12	0.18	5.54	4.43	3.68	1.72

[1] Note that $v_{RMS} = w_{RMS}$ due to our noise elimination procedure described in Section III which assumes the flow is statistically isotropic in the y-z plane.

Mean and RMS velocity

Although all the algorithms generate turbulence with a low mean flow (less than 1 cm/s in any given direction), it is preferable to normalize the mean velocities with their respective RMS velocities to compare the strength of the mean flow on a relative basis. Considering this parameter, the RANDOM and the different 4SECTRANDOM algorithms produce turbulence with the smallest mean flow in all directions. RANDOM (at x/M = 5.5 and 6.7) and 4SECTRANDOM2 (at the three downstream positions) generated the weakest mean flows (essentially 10% or less of the value of their respective RMS velocities in all directions). On the other hand, the chessboard-like and RANDOMNUMBER algorithms exhibited large relative mean flows (reaching values as high as 1.75 in the worst case). It was also observed that the RANDOMNUMBER algorithm resulted in values of $\langle U \rangle / u_{RMS}$ (velocity component normal to the plane of the RJA) being always higher than that of the other two components of the velocity (a trend not observed in any of the other algorithms tested). Although it is difficult to conclusively explain this observation using single-point Eulerian measurements as is the case herein, this may be due to a large number of jets operating during excessively long periods resulting in large $\langle U \rangle$ overall, which is consistent with the fact that the RANDOMNUMBER algorithm was characterized by the longest value of μ_{on} of all random algorithms, as well as large standard deviations.. Alternately expressed, such a scenario is possible given that the jets only change their state if the generated number is higher than the threshold, increasing the chances of jets maintaining their on state for a long time, as opposed to the other algorithms, which alternate the state of the jet in a "cyclical mode" at times defined by the on and off parameters (whose normal distributions reduce the possibility of excessively long intervals of jets operating).

As mentioned in section III, the noise correction of Khorsandi *et al.* (2012) for the RMS velocities was applied to improve the accuracy of the turbulence measurements. Due to the symmetry of the flow and the assumptions involved in the correction, w_{RMS} and v_{RMS} are thus identical. We note that u_{RMS} (normal to the jet array plane) is larger than w_{RMS} for 21 of the 23 cases examined herein. The higher values of u_{RMS} can possibly be attributed to it being the velocity component in the jet exit direction. We note that the measurements of Lavertu (2006) and

Khorsandi *et al.* (2013) are consistent with the present results undertaken in the same experimental facility. Moreover Variano and Cowen (2008) also observed the RMS of the velocity component in the direction normal to the plane of the RJA to be the largest. Regarding the 4SECTRANDOM class of algorithms, we observe that the RMS values increase with μ_{on} (4SECTRANDOM4 having the smallest μ_{on} and 4SECTRANDOM1 the largest). The same effect was observed during the exploration of variations of the RANDOM algorithms of Khorsandi (2011). The increase in the calculated RMS with μ_{on} may be attributed to the longer periods of injection of momentum, facilitating its propagation in the downstream direction, and favoring the development of longer "instantaneous gradients of velocity," allowing time for increased turbulent production. (See Variano and Cowen (2008), §5.3 for an extensive discussion of the effects of μ_{on}.) The 3 chessboard-based and the RANDOMNUMBER algorithms produce low RMS velocities, presumably caused by the large number of jets on at a given time, a drawback previously observed in RJAs. Variano and Cowen (2008) studied the effect of the average number of operating jets on the RMS velocities and found an optimal value over which additional (working) jets only serve to reduce the RMS velocities. In their RJA, the RMS velocities were maximized with 12.5% of pumps working, on average. Consistent with this finding, in our experimental facility the RANDOM and 4SECTRANDOM4 algorithms generate flows with the largest RMS velocities with (on average) 10% of the pumps on.

Isotropy, skewness and kurtosis

The isotropy of the flows is first quantified comparing the ratio w_{RMS}/u_{RMS} (Table 2). As already noted, we find that u_{RMS} is generally larger than w_{RMS} for almost all combinations of driving algorithm and downstream position. The flows generated by the chessboard patterns and the RANDOMNUMBER algorithms have better isotropy (close to one in some cases). The isotropy of the flows generated by the 4SECTRANDOM algorithms seems to be somewhat altered by changing the values of μ_{on}. The anisotropy observed using the RANDOM and 4SECTRANDOM algorithms is not entirely surprising. It presumably arises from the asymmetric forcing (from only one side of the tank), and has previously been observed in turbulent flows produced by random jet arrays (Variano and Cowen, 2008;

Khorsandi *et al.* 2013) as well as in active grid generated turbulence (Makita, 1991; Mydlarski and Warhaft, 1996). Lastly, the isotropy is observed to increase slightly with increasing distance from the jet array for most of the algorithms investigated, similar to that observed by Khorsandi *et al.* (2013). Essentially, the anisotropy resulting from the generation of the turbulence by the jets is gradually "forgotten" as the flow returns to isotropy away from the RJA. Bellani and Variano (2014), who used two RJAs facing each other, also observed that the isotropy improved in the central region of their tank. Hence, the additional symmetry of their bi-planar RJA system reduces the effect of the decay away from a single RJA and thus improves the isotropy of the flow.

The skewness ($S_\alpha = \langle\alpha^3\rangle/\langle\alpha^2\rangle^{3/2}$) quantifies the asymmetry of the distribution of velocity fluctuations. A negative skewness implies that negative fluctuations are more probable than positive ones, and conversely for positive skewness. The calculated values of S_v and S_w are close to zero (indicating essentially equal contributions from positive and negative fluctuations) and is effectively unaltered by the algorithm considered. Given the symmetry of the RJA, such results i) are expected, and ii) validate the statistically homogeneous nature of the flow in planes parallel to the RJA. S_u is found to be positive and order 1 for all the algorithms tested. Similarly, Variano and Cowen (2008) obtained a skewness of the velocity component normal to the plane of the RJA of 1.04. The non-zero skewness of a velocity component is apparently an unavoidable feature of the jet array that presumably results from the unidirectional forcing in the tank and subsequent decay of the turbulence in one direction. The injection of momentum occurs from the jet array and propagates in the downstream direction. Related to this argument, Maxey (1987) and Variano and Cowen (2008) claimed that in nearly homogeneous turbulence, in which the turbulent kinetic energy (TKE) decays in a given direction (e.g. downstream of a grid or RJA), there is a turbulent flux of TKE from the regions of higher TKE to lower TKE leading to a non-zero velocity skewness.

The kurtosis ($K_\alpha = \langle\alpha^4\rangle/\langle\alpha^2\rangle^2$) quantifies the importance of the tails of the distribution of velocity fluctuations, such that a high kurtosis is associated with frequently occurring large fluctuations. (A Gaussian distribution exhibits K=3.) Although, large fluctuations may not be desirable in certain situations (e.g. inertial

effects becoming important in particle dispersion due to strong and large displacements, or excessive flapping of a scalar source released into a flow), they do not result in anisotropies unless the kurtoses of the different velocity components are unequal. The RANDOM algorithm produces a flow with smaller and approximately similar kurtoses (in the three directions), which are nevertheless super-Gaussian. Other algorithms have higher kurtoses that are considerably different in the 3 directions and are thus, in that sense, less isotropic. Moreover, although effectively Gaussian statistics (S = 0, K = 3) are often defined in the study of homogeneous flows, probability distribution functions of velocity fields with super-Gaussian characteristics are relevant to other areas of fluid mechanics, such as the complex intermittent wind fields in which wind turbines operate (e.g. Good and Warhaft, 2011).

Turbulent kinetic energy (TKE)

The turbulent kinetic energy per unit mass (tabulated in Table 2 and plotted in Figure 5) is defined as $\frac{1}{2}(\langle u^2 \rangle + \langle v^2 \rangle + \langle w^2 \rangle)$ and used to quantify the intensity of the turbulence at various downstream distances, for the algorithms investigated herein. One observes that all the algorithms with a chessboard configuration produce low levels of TKE. The lower values associated with these algorithms presumably result from the large number of jets operating at a given time (50% of jets on), which reduces the RMS velocities. Variano and Cowen (2008) found that for their RJA, the RMS velocities were maximized with 12.5% of working jets on average. Hence, having 50% of the jets on at a given time (as is the case for this class of chessboard algorithms) may result in insufficient velocity differences/fluctuations, and be the cause of the low TKE. An intermediate level of turbulence was created using the RANDOMNUMBER algorithm. The RANDOM and 4SECTRANDOM series of algorithms produce the highest values of TKE, again resulting from the lower (but not too low) number of working jets (10% on average).

The TKE was also found to increase with increasing mean on times of the jets for the 4SECTRANDOM series of algorithms. RANDOM and 4SECTRANDOM1 produce the turbulence with the highest TKE for a given downstream distance (~10 cm^2/s^2 at x/M = 5.5). The TKE resulting from

4SECTRANDOM1 is about 30% higher than that in RANDOM, but exhibits a larger mean flow and anisotropy (Table 2). The higher mean flow may be a consequence of the imposition of the same number of jets operating in all quadrants (in the 4SECTRANDOM series of algorithms), which reduces the randomness and therefore possibly generate larger mean flows. Furthermore, an increased mean flow can advect the effects of individual jets (originating from the RJA) farther downstream, resulting in the measured increased anisotropy.

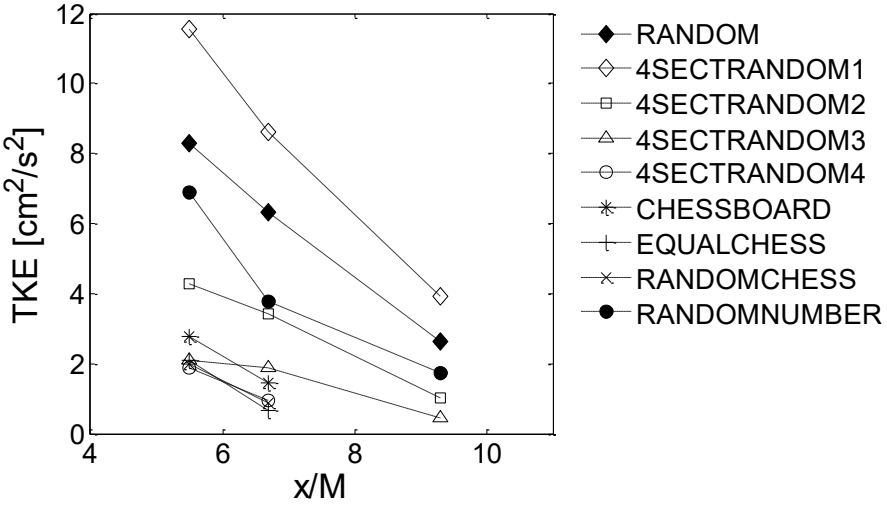

Figure 5. Evolution of the TKE with downstream distance.

Evaluation of the algorithms

As previously noted, the optimal algorithm should generate approximately homogeneous isotropic turbulence in our tank with a zero mean flow. Additionally, high levels of turbulence are desirable (as quantified by a large value of turbulent kinetic energy) to achieve Reynolds numbers that are more representative of "real" flows. The requirement of a negligible mean flow eliminates the algorithms of the chessboard type, as they create mean flows as large as 175% of the value of the RMS velocity. However, it should be noted that these algorithms are the least anisotropic. Consequently, these algorithms would be suitable for investigations in which the mean flow and high levels of turbulence are not significant limitations, but isotropy is an important requirement. Furthermore, if we restrict the strength of the mean flow to be less than 10% of the RMS value in all the directions, only 4SECTRANDOM2 and RANDOM (at x/M = 5.5 and 6.7) can be considered as

possible optimal algorithms, with the latter exhibiting a marginally smaller average mean flow (averaged over the *absolute value of the mean flow* for the nine cases corresponding to the three flow directions and three downstream positions) of 7% as compared to 8% for 4SECTRANDOM2. For these two cases, the isotopy (w_{RMS}/u_{RMS}) fell in the range of 0.62-0.77 for the RANDOM driving algorithm and in the range of 0.63-0.71 for the 4SECTRANDOM2 algorithm.

The TKE generated using the RANDOM algorithm is higher than that of 4SECTRANDOM2. Additionally, the turbulence generated using the RANDOM algorithm apparently decays at a slower rate than that created by 4SECTRANDOM2 (see Figure 6) when considering the decay in physical space, which is indeed the relevant case in the present context (as opposed to characterizing the decay as a function of eddy turnover time, for example). Furthermore, the TKE at x/M=9.3 using the RANDOM algorithm has decreased to 32% of its value at x/M=5.5 while for 4SECTRANDOM2 the TKE has decreased to 24% of its respective value at x/M=5.5. As previously noted, none of the algorithms studied herein eliminated the non-zero skewness in the x-component of the velocity (1.09-1.42 for RANDOM and 1.42-1.86 for 4SECTRANDOM2), suggesting that it is characteristic of all mono-planar RJA systems (as compared with the bi-planar system presented by Bellani and Variano, 2014). Also, the kurtoses are higher than that of a Gaussian distribution (K=3) for all the algorithms tested, however, it is the closest to the Gaussian value in all directions when using the RANDOM driving algorithm (average over the nine cases of 4.80, as compared to 6.08 for 4SECTRANDSOM2). Hence, we conclude that our optimal driving algorithm is RANDOM, as it generates turbulence with negligible mean flow (less than 10% the RMS value in all directions at x/M=5.5 and 6.7), high turbulent kinetic energy, and an acceptable degree of isotropy (especially when compared with the other algorithms tested).

Author accepted version. Final publication as:
Perez-Alvarado, A., Mydlarski, L.M., Gaskin, S.J. (2016) Effect of the driving algorithm on the turbulence generated by a random jet array, Experiments in Fluids, 57(2): 1-15. doi:10.1007/s00348-015-2103-7

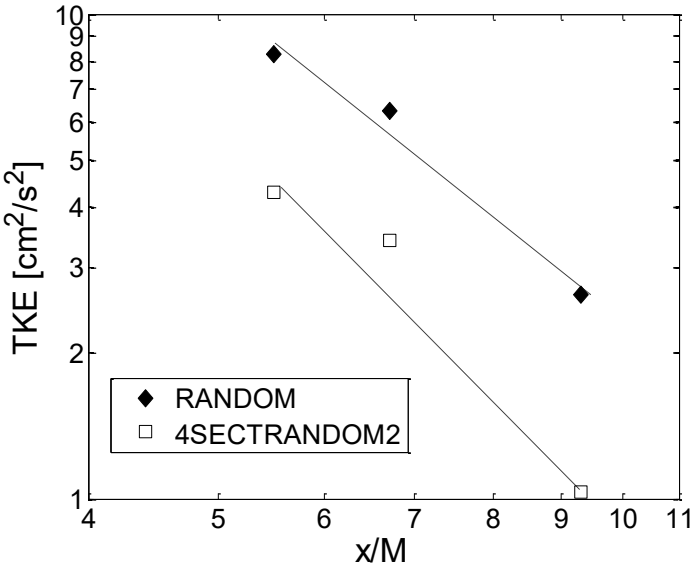

Figure 6. Downstream evolution of TKE for the RANDOM and 4SECTRANDOM2 algorithms.

The turbulent Reynolds number ($Re_T = u_T \ell/\nu$) was also calculated (see table 3), where ℓ is the integral length scale of the flow and u_T is a characteristic RMS velocity. ℓ is calculated from the spatial autocorrelation function ($\rho(r)$) of the y-component of the velocity. To be able to measure ℓ, the ADV probe was translated at a constant speed (0.2 m/s) in the y-direction. The spatial autocorrelation was subsequently calculated assuming Taylor's hypothesis, which was valid given that the translation velocity was an order of magnitude larger than the characteristic RMS velocity. The spatial autocorrelation functions ($\rho(r)$) used for the calculation of ℓ at the three downstream positions are plotted in figure 7. To account for the slight anisotropy in the velocity components, we calculated a characteristic velocity $u_T = (1/3(u^2_{RMS} + v^2_{RMS} + w^2_{RMS}))^{1/2}$ following the definition used by Variano and Cowen (2008) for their RJA.

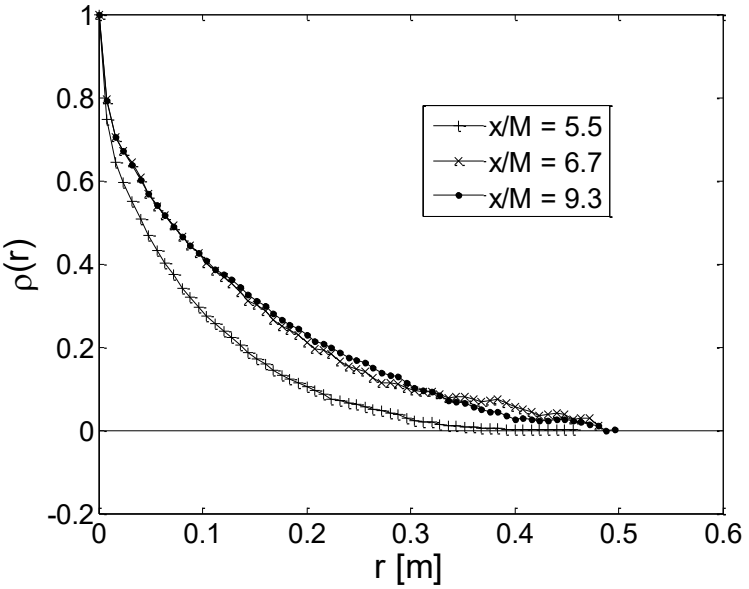

Figure 7. Spatial autocorrelations at different distances from the RJA.

The fact that Re_T reaches its highest value at x/M = 6.7 may imply that the flow is still under development at x/M = 5.5. This result is consistent with the description of a jet-merging region extending up to x/M = 6, as suggested by Variano and Cowen (2008). Furthermore, the little change in ℓ between x/M=6.7 and x/M = 9.3 supports the idea that the flow is still developing at x/M = 5.5. Thus, we recommend that the measurements in investigations using the turbulent flow generated by RANDOM should be performed at positions farther downstream than x/M=5.5, although more measurements would be necessary to fully quantify the evolution of the flow downstream of the RJA.

Table 3. Characteristic velocity (u_T), integral length scale (ℓ) and Re_T for the flow generated using the RANDOM algorithm. $\nu = 1x10^{-6}$ m^2/s.

Algorithm	x/M	u_T [cm/s]	ℓ [cm]	$Re_T \equiv u_T \ell/\nu$
RANDOM	5.5	2.35	7.5	1760
	6.7	2.05	11.5	2360
	9.3	1.33	11.6	1540

We compare the results of the flow generated by the RANDOM algorithm with previous investigations in Table 4. The results show that our system performs quite well when compared with other ones. Although the mean flow in our system is not zero, it was lower than that in most previous similar systems. The integral length scale (ℓ) in our flow is the largest reported. Our ratio ℓ/M = 0.77 at x/M = 6.7

is almost the same as the value of $\ell/M = 0.76$ of Variano and Cowen (2008) at $x/M = 6.0$, which may be interpreted as a sign of the similarity in the development of the two flows despite the larger scale of our facility. A large integral length scale can be useful for the study of the effects of large scales in turbulence. Moreover, along with the Re, large values of ℓ allow the existence of an inertial subrange covering a broad range of (readily measurable) scales. The anisotropy in Table 4 corresponds to the lowest ratio of RMS velocities measured at the center of the experimental facilities (in our study it is w_{RMS}/u_{RMS}). Although some studies reported the variation of the ratio of the RMS velocities in a central plane, others reported the values at the center of their tank, thus for a fair comparison the values used in Table 4 are those measured at the center of the apparatuses. The moderate anisotropy in our system is its largest drawback. However, it could be eliminated by converting our system into a double RJA, by the addition of a second RJA facing our existing one. The Reynolds number in our system is one of the highest reported to date and comparable to that of other RJAs (Variano and Cowen, 2008, and Bellani and Variano, 2014). The homogeneity of the flow in planes parallel to the RJA covers a large area of approximately 0.75×0.75 m^2 (see Khorsandi (2011)). Such a large homogeneous region cannot be achieved in most other types of systems, and it is thus encouraging that a relatively high quality turbulent flow was generated in a facility of this size. The approximately zero-mean-flow homogeneous isotropic turbulence generated by our large random jet array proves the flexibility of RJAs to be scaled to study turbulent flows at larger scales.

Author accepted version. Final publication as:
Perez-Alvarado, A., Mydlarski, L.M., Gaskin, S.J. (2016) Effect of the driving algorithm on the turbulence generated by a random jet array, Experiments in Fluids, 57(2): 1-15. doi:10.1007/s00348-015-2103-7

Table 4. Comparison with other studies of zero-mean-flow, homogeneous isotropic turbulence.

System	Max ($\langle U_\alpha \rangle / u_{\alpha_{RMS}}$)	ℓ [cm]	Anisotropy ($u_{\alpha_{RMS}} / u_{\beta_{RMS}}$)	Re_T	Reference
Single RJA	0.08	7.5	0.62	1760	Present work, RANDOM at *x*/M=5.5
Single RJA	0.05	11.5	0.63	2360	Present work, RANDOM at *x*/M=6.7
Single RJA	0.2	11.6	0.77	1540	Present work, RANDOM at *x*/M=9.3
Single RJA	0.07	7.6	0.79	3220	Variano and Cowen (2008) at *x*/M=6
Facing dual RJA	0.1	9.5	0.95	2000	Bellani and Variano (2014)
Two oscillating grids	0.3	2.2	0.9	75	Srdic *et al.* (1996)
Two oscillating grids	0.28	0.3	0.9	55	Shy *et al.* (1997)
Rotating grids	0.7	4.7	0.85	2540	Liu *et al.* (1999)
Propellers	0.1	6	0.9	504	Zimmermann *et al.* (2010)
Loudspeakers	0.1	2.8	0.97	1590	Hwang and Eaton (2004)
Loudspeakers	0.04	3.6	0.95	2040	Goepfert *et al.* (2010)
Loudspeakers	0.04	9.9	0.94	4230	Chang *et al.* (2012)

VI. Conclusions

Different driving algorithms for a planar random jet array were tested to compare the statistics of the generated turbulence downstream of the RJA in an attempt to both further characterize their performance and find an optimal algorithm that approximates zero-mean-flow homogeneous isotropic turbulence. The algorithm identified as RANDOM generated a flow with relatively high turbulent kinetic energy and the most closely approximated zero-mean-flow homogeneous isotropic turbulence (on an overall basis), exhibiting variations in horizontal and vertical homogeneity of no more than ±6%, and mean flows of 7% of the RMS velocities averaged over (the absolute value of the) three velocity components and three downstream distances measured herein. The measured anisotropy (w_{RMS}/u_{RMS} in the range of 0.62-0.77) was not negligible, but could be reduced at the expense of other desirable characteristics of the flow (e.g. Reynolds number/downstream position; zero mean flow). Also, it should be noted that all of the tested algorithms produced non-zero skewness of the fluctuating velocity normal to the plane of the RJA, as well as super-Gaussian kurtoses of all the three components of velocity. This is identified as an inherent limitation of the system resulting from the unidirectional forcing imposed from only one side of the RJA. This non-zero skewness could be overcome (at least at the center of the tank) by placing two RJAs facing each other such as the apparatus built by Bellani and Variano (2014). The results of Bellani and Variano (2014) showed that the isotropy is improved in a

relatively large central section of the tank, however, the evolution of the skewness and kurtosis of the velocity components was not discussed. Our RANDOM algorithm (also called the "sunbathing" algorithm) generates turbulent flow with a relatively high Reynolds number (Re_T = 2360) and the largest reported integral length scale (ℓ = 11.5 cm) for a random jet array. These results validate the versatility of random jet arrays and their ability to be scaled up and continue to generate approximately homogeneous isotropic flow with negligible mean flow. Lastly, the present tabulation and review of the 9 driving algorithms studied herein, including those not deemed optimal, may be used by future researchers who require certain specific characteristics in a flow (e.g. large kurtosis/high levels of intermittency) and who may be less concerned with those that were the focus of the present research (e.g. zero-mean flow).

Appendix. Sources of error and uncertainty analysis

The purpose of this section is to describe the potential sources of error and quantify their effect on the results. It is important to note that the total uncertainty arises from the i) ADV uncertainty, and ii) propagation of the ADV uncertainties due to the corrections performed. The analysis that follows considers each potential source of error in the velocity measurements conducted by acoustic Doppler velocimetry. The uncertainty analysis models of Voulgaris and Trowbridge (1998) and Taylor (1997) are used to estimate the uncertainty. The sources of error are then combined to calculate the uncertainty in each component of the velocity. Finally, the total relative uncertainty resulting from the propagation of the ADV uncertainty is calculated.

A.1 Acoustic Doppler velocimetry uncertainties

Voulgaris and Trowbridge (1998) identified three sources of error for the total velocity along each receiver beam (σ_t): i) sampling error (σ_m), caused by the inability of the system to resolve the phase shift of the return pulse, ii) Dopler noise

(σ_D), due to random scatter motions within the sample volume, and iii) error resulting from the mean velocity shear within the sampling volume (σ_u). σ_u becomes important in the presence of sharp velocity gradients (e.g. in boundary or mixing layers). However, in homogeneous flows like those produced by our algorithms, the mean velocity gradients are negligible far enough from the RJA. Thus, the mean velocity shear error was neglected in our calculations. In the following sections the sampling and Doppler errors are calculated individually. The calculations are made for the RANDOM algorithm at the three downstream positions investigated (similar results are obtained for the other algorithms, but not presented herein).

A.1.1 Sampling error

Sampling error results from the inaccuracy of the A/D converter (in the ADV system) in resolving the changes in phase of the return pulse and the noise induced by the electronics. This error is independent of the flow and depends on the velocity range employed when operating the ADV. During our experiments the ADV's ±0.3 m/s velocity range was used for the velocity measurements at x/M= 5.5 and 6.7, while the ±0.1 m/s velocity range was used for the measurements at x/M=9.3. The sampling error can be calculated as (Voulgaris and Trowbridge, 1998):

$$\sigma_m^2 = \frac{c^2}{4}\frac{1}{f^2}\frac{1}{4\pi^2}K^2\sigma_s^2\frac{1}{\tau}\frac{1}{(T-t_0)}\ ,$$

where c is the speed of sound in water (1481 m/s at 20 ˚C), f is the operating frequency of the ADV (10 MHz), K is an empirical constant (1.4, Zedel *et al.* 1996), σ_s^2 is the system's uncertainty to resolve the phase (1.08 and 0.63 for the ±0.3 and ±0.1 m/s velocity range, respectively), τ is the time between transmissions (4.35 and 5.55 ms for the ±0.3 and ±0.1 m/s velocity range, respectively), T is the inverse of the sampling frequency (0.04 s at a sampling frequency of 25 Hz), and t_0 is the time required by the system to carry out the necessary conversions (2 ms). The calculated sampling error is shown in the following table.

Table 5. Calculation of sampling error (σ_m^2).

Algorithm	x/M	ADV's velocity range (m/s)	σ_m^2 (m^2/s^2)

RANDOM	5.5	± 0.3	1.78E-06
	6.7	± 0.3	1.78E-06
	9.3	± 0.1	8.13E-07

A.1.2 Doppler noise

Doppler noise (an intrinsic feature in Doppler acoustic systems) is caused by: i) the finite residence time of the particles in the sampling volume, ii) turbulence within the sampling volume, and iii) beam divergence. Voulgaris and Trowbridge (1998) presented the following equations for the calculation of the Doppler noise (σ_D^2):

$$\sigma_D^2 = \frac{\pi^{-1/2}}{16}\frac{c^2 B_D}{f^2 M_{ADV}\,\tau}\ ,$$

where M_{ADV} (=11) is the number of acoustic pulses averaged for the calculation of the radial velocity, and B_D is the total Doppler bandwidth broadening. B_D is the RMS of the three individual contributions of the bandwidth broadening due to the (as mentioned above) finite residence time (B_r), turbulence within the sample volume (B_t), and the beam divergence (B_d):

$$B_D^2 = B_r^2 + B_t^2 + B_d^2\ .$$

B_r, B_t, and B_d can be calculated using the following expressions:

$$B_r = 0.2\frac{U_h}{d}\ ,$$

where U_h is the mean horizontal speed (i.e. $U_h = (\langle U\rangle^2 + \langle V\rangle^2)^{1/2}$) and d is the transverse size of the sampling volume.

$$B_t = 2.4\frac{f(\varepsilon d)^{1/3}}{c}\ ,$$

where ε is the turbulence dissipation rate (estimated from u^3/ℓ , where u is the characteristic velocity and ℓ is the integral length scale, both calculated in section V).

$$B_d = 0.84\sin(\Delta\theta)\frac{fU_c}{c}\ ,$$

where Δθ is the angle bisector between the transmitter and receiver (15˚ for our system), and U_c is the cross-beam or transverse velocity component ($\langle V\rangle$). The following table summarizes the quantities used to ultimately calculate σ_D^2:

Author accepted version. Final publication as:
Perez-Alvarado, A., Mydlarski, L.M., Gaskin, S.J. (2016) Effect of the driving algorithm on the turbulence generated by a random jet array, Experiments in Fluids, 57(2): 1-15. doi:10.1007/s00348-015-2103-7

Table 6. Calculation of the Doppler noise (σ_D^2)

Algorithm	x/M	B_r (1/s)	B_t (1/s)	B_d (1/s)	σ_D^2 (m^2/s^2)
RANDOM	5.5	3.5E-02	168.77	0.22	2.73E-06
	6.7	1.4E-02	127.64	0.11	2.06E-06
	9.3	9.6E-02	82.49	4.58	1.05E-06

A.1.3 Uncertainty for the acoustic Doppler velocimetry measurements.

The total uncertainty of the ADV measurements is calculated assuming random independent errors. It can be calculated using the following equation (Taylor, 1997):

$$Total\ Uncertainty\ = \sqrt{(Uncertainty_1)^2 + (Uncertainty_2)^2 + (Uncertainty_3)^2 + \cdots}$$

The total velocity uncertainty ($\sigma_{t\text{-}RMS}^2$) for the RMS velocity along each receiver beam of the ADV can then be calculated as the sum of the sampling error (σ_m^2) and the Doppler noise (σ_D^2). Recall that the error due to the mean velocity shear is negligible, thus $\sigma_{t\text{-}RMS}^2 = \sigma_m^2 + \sigma_D^2$, which is tabulated below:

Table 7. Calculation of the total velocity uncertainty for the RMS along each receiver ($\sigma_{t\text{-}RMS}^2$)

Algorithm	x/M	$\sigma_{t\text{-}RMS}^2$ (m^2/s^2)
RANDOM	5.5	4.51E-06
	6.7	3.84E-06
	9.3	1.86E-06

We can assume that σ_t^2 is the same along each receiver beam if the receiver transducers are identical and ideal. Under this assumption, the uncertainty of the RMS velocity for each velocity component ($\sigma_{i\text{-}RMS}^2$) can be calculated using the ADV's transformation matrix. The following table presents the uncertainties for the three RMS velocity components.

Table 8. Calculation of the total uncertainty for each velocity component ($\sigma_{i\text{-}RMS}^2$)

Algorithm	x/M	$\sigma_{x\text{-}RMS}^2$ (m^2/s^2)	$\sigma_{y\text{-}RMS}^2$ (m^2/s^2)	$\sigma_{z\text{-}RMS}^2$ (m^2/s^2)
RANDOM	5.5	3.71E-05	3.66E-05	2.40E-06
	6.7	3.16E-05	3.12E-05	2.05E-06
	9.3	1.53E-05	1.51E-05	9.90E-07

We note the smaller uncertainty for the z-component of velocity (w), as previously discussed, as well as in Khorsandi *et al.* (2012).

A.2 Propagation of uncertainties

As mentioned in section III, some corrections were applied to the calculated RMS velocities. The corrections included in some cases the combination of the three calculated RMS velocities resulting in a propagation of the uncertainties. The RMS velocity in the z-direction was not modified and thus the corresponding uncertainty remains the same as calculated in A.1.3 (i.e. $w_{\text{RMS}} = [\langle w^2 \rangle + \sigma_{z\text{-RMS}}{}^2]^{1/2}$). The RMS velocity in the y-direction was assumed to be the same as that of the z-direction due to the axisymmetric nature of the flow, then the uncertainty in v is the same as that of w (z-direction). On the other hand, the corrected RMS velocity in the x-direction was calculated using the three calculated RMS velocity components u_{RMS}, v_{RMS}, and w_{RMS} (each one with a corresponding uncertainty). The expression used in the correction of u_{RMS} (process described in section III) is the following:

$$u_{c-RMS} = \left[u_{RMS}^2 - \frac{(a_{11}^2 + a_{12}^2 + a_{13}^2 + a_{14}^2)}{(a_{21}^2 + a_{22}^2 + a_{23}^2 + a_{24}^2)} (v_{RMS}^2 - w_{RMS}^2) \right]^{1/2},$$

where $u_{\text{c-RMS}}$ is the corrected RMS velocity, and a_{ij} are elements of the transformation matrix. The total relative uncertainties for the RMS velocities were calculated performing a step-by-step analysis of uncertainty propagation (Taylor, 1997). The final results are presented in the following table:

Table 9. Calculation of the total relative uncertainties for the RMS velocity components.

Algorithm	x/M	% u_{RMS} error	% v_{RMS} error	% w_{RMS} error
RANDOM	5.5	2.81	0.33	0.33
	6.7	3.18	0.37	0.37
	9.3	4.49	0.35	0.35

The table above shows that the total relative uncertainty for the RMS velocity is less than 5% in any given direction, being the largest for the u-component of the velocity.

References

Aumaitre, S., Fauve, S. and Pinton, J. F. 2000. Large scale correlations for energy injection mechanisms in swirling turbulent flows. *Eur. Phys. J.* B 16, 563-567.

Belin, F., Maurer, J., Tabeling, P. and Willaime, H. 1997. Velocity gradient distributions in fully developed turbulence: An experimental study. *Phys. Fluids* 9, 3843-3850.

Bellani, G. and Variano, E.A. 2014. Homogeneity and isotropy in a laboratory turbulent flow. *Exp. Fluids* (2014) 55:1646.

Berg, J., Luthi, B., Mann, J. and Ott, S. 2006. Backwards and forwards relative dispersion in turbulent flow: an experimental investigation. *Phys. Rev. E* 74, 016304.

Birouk, M., Sarh, B., and Gokalp, I. 2003. An attempt to realize experimental isotropic turbulence at low Reynolds number. *Flow Turbul. Combust.* 70:325–348.

Blum, D. B., Kunwar, S. B., Johnson, J. and Voth, G. A. 2010. Effects of nonuniversal large scales on conditional structure functions in turbulence. *Phys. Fluids* 22, 015107.

Blum, D. B., Bewley, G. P., Bodenschatz, E., Gibert, M., Gylfason, A., Mydlarski, L., Voth, G. A., Xu, H., and Yeung, P. K. 2011 Signatures of non-universal large scales in conditional structure functions from various turbulent flows. *New J. Phys.* 13, 113020.

Bodenschatz, E., Bewley, G. P., Nobach, H., Sinhuber, M., and Xu, H. 2014. Variable density turbulence tunnel facility. *Review of Scientific Instruments* 85,093908 (2014)

Brumley, B. H. and Jirka, G. H. 1987. Near-surface turbulence in a grid-stirred tank. *J. Fluid Mech.*183, 235–263.

Cadot, O., Douady, S. and Couder, Y. 1995. Characterization of the low-pressure filaments in a three-dimensional turbulent shear flow. *Phys. Fluids* 7, 630-646.

Chang, K., Bewley, G. P. and Bodenschatz, E. 2012. Experimental study of the influence of anisotropy on the inertial scales of turbulence. *J. Fluid Mech.* 692:464–481

De Jong, J., Cao, L., Woodward, S., Salazar, J., Collins, L., and Meng, H. 2008. Dissipation rate estimation from PIV in zero-mean isotropic turbulence. *Exp. Fluids,* 46:499–515

De Silva, I.P.D. and Fernando, H.J.S. 1994. Oscillating grids as a source of nearly isotropic turbulence. *Phys. Fluids* 6, 2455-2465.

Delbos, S., Weitbrecht V., Bleninger T., Grand P. P., Chassaing E., Lincot D., Kerrec O., and Jirka G. H. 2009. Homogeneous turbulence at an electrodeposition surface induced by randomly firing jet arrays. *Exp. Fluids*, 46, 1105.

Douady, S., Couder, Y., and Brachet, M. E. 1991. Direct observation of the intermittency of intense vorticity filaments in turbulence. *Phys. Rev. Lett.* 67(8):983–986.

Fallon, T., and Rogers, C. B. (2002) Turbulence-induced preferential concentration of solid particles in microgravity conditions. *Exp. Fluids,* 33:233–241.

Fauve, S., Laroche, C. and Castaing, B. 1993. Pressure fluctuations in swirling turbulent flows. *J. Phys.* Paris II 3, 271-278.

Fernando, H.J.S. and De Silva, I.P.D. 1993. Note on secondary flows in oscillating-grid, mixing-box experiments. *Phys. Fluids*, A5 (7): 1849-1851.

Goepfert, C., Marie´, J., Chareyron, D., and Lance, M. 2010. Characterization of a system generating a homogeneous isotropic turbulence field by free synthetic jets. *Exp. Fluids,* 48:809–822

Good, G. H. and Warhaft, Z., 2011. On the probability distribution function of the velocity field and its derivative in multi-scale turbulence. *Phys. Fluids* 23(9), 095106.

Hwang, W., and Eaton, J. K. 2004. Creating homogeneous and isotropic turbulence without a mean flow. *Exp. Fluids,* 36:444–454

Khorsandi, B., 2011. PhD Thesis. Effect of background turbulence on an axisymmetric turbulent jet.

Khorsandi, B., Mydlarski, L. and Gaskin, S. J., 2012. Noise in turbulence measurements using acoustic Doppler velocimetry. *J. Hydraul. Eng.* vol. 138 No. 10, pp. 829-838.

Khorsandi, B., Gaskin, S. and Mydlarski, L., 2013. Effect of background turbulence on an axisymmetric turbulent jet. *J. Fluid Mech.* 736, pp. 250-286.

Lavertu, T. M. 2006. Differential diffusion in a turbulent jet. PhD thesis, McGill University.

Liu, S., Katz, J., and Menevau, C. 1999. Evolution and modelling of subgrid scales during rapid straining of turbulence. *J. Fluid Mech.* 387:281–320

Lu, J., Fugal, J. P., Nordsiek, H., Saw, E. W., Shaw, R. A. and Yang, W. 2008. Lagrangian particle tracking in three dimensions via single-camera in-line digital holography. *New J. Phys.* 10,125013.

Machicoane, N., Zimmermann, R., Fiabane, F., Bourgoin, M., Pinton, J.-F. and Volk, R. 2014. Large sphere motion in a nonhomogeneous turbulent flow. *New J. Phys.* 16, 013053.

Makita, H. 1991. Realization of a large-scale turbulence field in a small wind tunnel. *Fluid Dyn. Res.* 8:53–64.

Maurer, J., Tabeling, P. and Zocchi, G. 1994. Statistics of turbulence between two counter-rotating disks in low-temperature helium gas. *Europhys. Lett.* 26, 31-36.

Maxey, M.R. 2007. The velocity skewness measured in grid turbulence. *Phys. Fluids*, v 30, n 4, p 935-8.

McDougall, T.J. 1979. Measurements of turbulence in a zero-mean shear mixed layer. *J. Fluid Mech.* 94 (3): 409–431.

McKenna, S.P. and McGillis, W.R. 2004. Observations of flow repeatability and secondary circulation in an oscillating grid-stirred tank. *Phys. Fluids*, 16 (9): 3499-3502.

McLelland, S. J., and Nicholas, A. P. 2000. A new method for evaluating errors in a high-frequency ADV measurements. *Hydrol. Processes*, 14(2), 351–366.

Mordant, N., Metz, P., Michel, O. and Pinton, J. 2001. Measurement of Lagrangian velocity in fully developed turbulence. *Phys. Rev. Lett.* 87, 214501.

Mydlarski, L. and Warhaft, Z. 1996. On the onset of high-Reynolds number grid-generated wind tunnel turbulence. *J. Fluid Mech.* 320:331–368.

Mydlarski, L. and Warhaft, Z. 1998. Passive scalar statistics in high-Péclet number grid turbulence. *J. Fluid Mech.* 358, pp 135-175

Liberzon, A., Guala, M., Lüthi, B., Kinzelbach, W., and Tsinober, A. 2005. Turbulence in dilute polymer solutions. *Phys. Fluids* 17, 031707.

Orszag, S. A. 1977. Lectures on the statistical theory of turbulence. In Fluid Dynamics (ed. R. Balian & J. L. Peube), p. 235. Gordon & Breach.

Ott, S. and Mann, J. 2000. An experimental investigation of the relative diffusion of particle pairs in three-dimensional turbulent flow. *J. Fluid Mech.* 422, 207.

Shy, S. S., Tang, C. Y., and Fann, S. Y. 1997. A nearly isotropic turbulence generated by a pair of vibrating grids. *Exp. Thermal Fluid Sci.* 14:251–262

Srdic, A., Fernando, H.J.S., and Montenegro, L. 1996. Generation of nearly isotropic turbulence using two oscillating grids. *Exp. Fluids,* 20:395–397

Taylor, J. R., 1997. An Introduction to Error Analysis. University Science Books.

Thompson, S. and Turner, J. S. 1975. Mixing across an interface due to turbulence generated by an oscillating grid. *J. Fluid Mech.* 67, 349-368.

Tsinober, A. 2004. An informal introduction to turbulence. Kluwer Academic Publisher.

Villermaux, E., Sixou, B., and Gagne, Y. 1995. Intense Vortical Structures in Grid-Generated Turbulence. *Phys. Fluids,* 7(8), 2008-2013.

Variano, E. A., Bodenschatz, E., and Cowen, E. A. 2004. A random synthetic jet array driven turbulence tank. *Exp. Fluids,* 37:613–615

Variano, E. A., and Cowen E. A. 2008. A random-jet-stirred turbulence tank. *J. Fluid Mech.* 604:1–32

Vectrino Velocimeter User Guide, Nortek, 2004.

Voulgaris, G. and Trowbridge, J. H. 1998. Evaluation of the acoustic Doppler velocimeter (ADV) for turbulence measurements. *J. Atmos. Oceanic Tech.* 15: 272-289.

Voth G., Porta A. L., and Crawford A. 2002. Measurement of particle accelerations in fully developed turbulence. *J. Fluid Mech.* 469:121–160

Warnaars, T. A., Hondzo, M. and Carper, M. A. 2006. A desktop apparatus for studying interactions between microorganisms and small-scale fluid motion. *Hydrobiologia,* 563, 431–443.

Webster, D. R., Brathwaite, A. and Yen, J. 2004. A novel laboratory apparatus for simulating isotropic oceanic turbulence at low Reynolds number. *Limnol. Oceanogr. Methods,* 2, 1–12.

Zedel, L., Hay, A. E., Cabrera, R., and Lohrmann, A. 1996. Performance of a single- beam pulse-to-pulse coherent Doppler profiler. *IEEE Journal of Oceanic Engineering*, vol.21, no.3, pp. 290-297.

Zimmermann, R., Xu, H., Gasteuil, Y., Bourgoin, M., Volk, R., Pinton, J.F., and Bodenschatz, E. 2010. The Lagrangian exploration module: an apparatus for the study of statistically homogeneous and isotropic turbulence. *Rev. Sci. Instrum.* 81:055112